Climate Dynamics (2006) 27: 593–611
DOI 10.1007/s00382-006-0151-7

P. D. Williams · E. Guilyardi · R. T. Sutton
J. M. Gregory · G. Madec

On the climate response of the low-latitude Pacific Ocean to changes in the global freshwater cycle

Received: 24 June 2005 / Accepted: 29 March 2006 / Published online: 19 May 2006

Abstract Under global warming, the predicted intensification of the global freshwater cycle will modify the net freshwater flux at the ocean surface. Since the freshwater flux maintains ocean salinity structures, changes to the density-driven ocean circulation are likely. A modified ocean circulation could further alter the climate, potentially allowing rapid changes, as seen in the past. The relevant feedback mechanisms and timescales are poorly understood in detail, however, especially at low latitudes where the effects of salinity are relatively subtle. In an attempt to resolve some of these outstanding issues, we present an investigation of the climate response of the low-latitude Pacific region to changes in freshwater forcing. Initiated from the present-day thermohaline structure, a control run of a coupled ocean–atmosphere general circulation model is compared with a perturbation run in which the net freshwater flux is prescribed to be zero over the ocean. Such an extreme experiment helps to elucidate the general adjustment mechanisms and their timescales. The atmospheric greenhouse gas concentrations are held constant, and we restrict our attention to the adjustment of the upper 1,000 m of the Pacific Ocean between 40°N and 40°S, over 100 years. In the perturbation run, changes to the surface buoyancy, near-surface vertical mixing and mixed-layer depth are established within 1 year. Subsequently, relative to the control run, the surface of the low-latitude Pacific Ocean in the perturbation run warms by an average of 0.6°C, and the interior cools by up to 1.1°C, after a few decades. This vertical rearrangement of the ocean heat content is shown to be achieved by a gradual shutdown of the heat flux due to isopycnal (i.e. along surfaces of constant density) mixing, the vertical component of which is downwards at low latitudes. This heat transfer depends crucially upon the existence of density-compensating temperature and salinity gradients on isopycnal surfaces. The timescale of the thermal changes in the perturbation run is therefore set by the timescale for the decay of isopycnal salinity gradients in response to the eliminated freshwater forcing, which we demonstrate to be around 10–20 years. Such isopycnal heat flux changes may play a role in the response of the low-latitude climate to a future accelerated freshwater cycle. Specifically, the mechanism appears to represent a weak negative sea surface temperature feedback, which we speculate might partially shield from view the anthropogenically-forced global warming signal at low latitudes. Furthermore, since the surface freshwater flux is shown to play a role in determining the ocean's thermal structure, it follows that evaporation and/or precipitation biases in general circulation models are likely to cause sea surface temperature biases.

P. D. Williams (✉) · E. Guilyardi · R. T. Sutton · J. M. Gregory
Centre for Global Atmospheric Modelling,
Department of Meteorology, University of Reading,
PO Box 243, Earley Gate, Reading RG6 6BB, UK
E-mail: p.d.williams@reading.ac.uk
Tel.: +44-118-3787901
Fax: +44-118-3788316

E. Guilyardi
Laboratoire des Sciences du Climat et de l'Environnement
(IPSL/LSCE), Gif-sur-Yvette, France

J. M. Gregory
Hadley Centre for Climate Prediction and Research, Exeter, UK

G. Madec
Laboratoire d'Océanographie et de Climat par
Expérimentation et Approche Numérique (IPSL/LOCEAN),
Université Paris VI, Paris, France

1 Introduction

An intensified global freshwater cycle (i.e. hydrological cycle) is a likely consequence of global warming (Bosilovich et al. 2005). This is because basic atmospheric thermodynamics predicts that a warmer surface increases the rates of evaporation and evapotranspiration (for a given surface wind speed), and that a warmer

atmosphere can attain greater absolute humidities. These predictions are in accordance with the observational evidence presented by Gaffen et al. (1991) that the tropical tropospheric water vapour content has increased since the mid-1970s. Averaged over the globe, and over timescales longer than the mean residence time of water vapour in the atmosphere [calculated to be around 10 days by Chahine (1992)], any increase in evaporation must be balanced by a similar increase in precipitation to remain in a steady state.

As evidence that the processes described above are already taking place in the climate system, Dai et al. (1997) have reported observations of a linear increasing trend in global precipitation over land between 1900 and 1988, of magnitude around 2.4 mm decade^{-1}. Spatially, this trend is fairly uniform in the mid- and high-latitudes, although it is negative in some low-latitude regions. Wong et al. (1999) have inferred an increase in high-latitude precipitation over the Pacific Ocean between the period 1930–1980 and the period 1985–1994, from measurements of the salinity of intermediate waters. Russell et al. (1995) have reported a global precipitation increase (of around 3.0 mm decade^{-1}) in a 1% year^{-1} CO_2 scenario run using a coupled ocean–atmosphere general circulation model (GCM); such increases are predicted by almost all coupled GCMs (IPCC 2001). Future changes to both the magnitudes and the spatial patterns of the atmosphere–ocean–land freshwater fluxes are therefore likely consequences of global warming, although the ocean component of the water cycle remains poorly understood (Schmitt 1995).

The global hydrological cycle leaves a salinity signature in the ocean. Salinity structures are forced at the surface by freshwater exchange with the atmosphere (evaporation and precipitation), the land (river run-off) and sea-ice (formation or melting). Ocean salinity therefore has a very different distribution from that of temperature, which is forced by differences in heat exchange with the atmosphere, especially between the equator and the poles. Furthermore, there is a rapid negative feedback between sea surface temperature (SST) anomalies and surface heat flux anomalies, but there is no such feedback between sea surface salinity (SSS) anomalies and surface freshwater flux anomalies. SST and SSS anomalies are therefore dissipated on very different timescales (e.g., Spall 1993; Hall and Manabe 1997). At high-latitudes, where the temperature range with depth is much smaller than at low latitudes, and where the effect on density of a given salinity anomaly is greater because of the lower mean temperature, salinity plays a crucial role in setting the vertical stability, and is therefore a major driver of the global thermohaline circulation (Rahmstorf 1996; Saenko et al. 2002). At lower latitudes the effects of salinity are more subtle, but significant impacts can arise through its roles in defining surfaces of constant density, along which enhanced advection and diffusion occur, and in defining barrier layers (Maes et al. 2005).

Under global warming, any changes to the hydrological cycle will modify ocean salinity. Observations of freshening in the Pacific and Indian oceans have been reported by Bindoff and McDougall (2000) and Banks and Bindoff (2003). Modified salinity structures could potentially alter the ocean circulation, through their impact on density. A modified ocean circulation could further alter the climate (e.g., Dong and Sutton 2002; Vellinga and Wood 2002), potentially allowing rapid climatic changes, as seen in the past in palaeoclimate records from long Greenland ice cores (e.g., Broecker et al. 1985). This feedback loop is summarized in Fig. 1. Furthermore, the global freshwater transport is less strongly constrained by radiative forcing than the global heat transport (Allen and Ingram 2002). The ocean salinity field may therefore have more degrees of freedom with which to respond to changes in greenhouse gas (GHG) forcing than does the temperature field. For these reasons, processes involving salinity may be crucial in determining the response of the climate to anthropogenic GHG emissions.

Despite the vital role played by salinity in ocean circulation and climate, the feedback mechanisms (and timescales) that maintain the salinity structure are poorly understood in detail. Insight into the processes that determine the mean salinity distribution, and its variability, has therefore remained elusive. Part of the difficulty stems from the coupled nature of the problem: interactions between the ocean and atmosphere, both in the tropics and at high-latitudes, are key processes, as is the transport of water vapour within the atmosphere (both meridional and inter-basin) and high-latitude

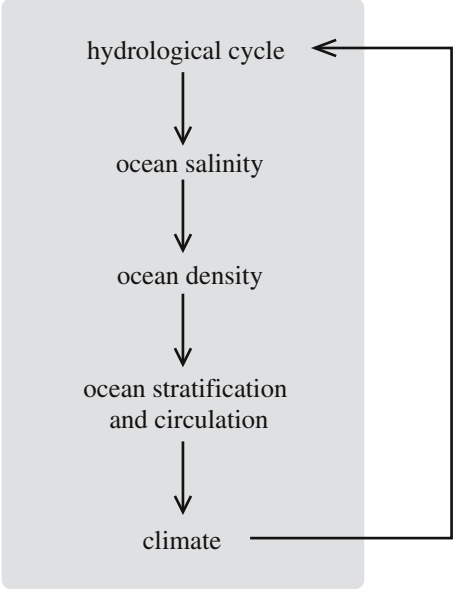

Fig. 1 Feedback loop illustrating how not only may the climate influence the hydrological cycle, as discussed in the text, but also the hydrological cycle may influence the climate. It is the latter part of this loop (shown *shaded*), in which ocean salinity plays a crucial role, that is the subject of this study

interaction with sea-ice. Furthermore, because of the technical difficulties of measuring salinity (and precipitation/evaporation over ocean), there are relatively few observations with which to validate models.

In an attempt to resolve some of these outstanding issues, this paper aims to investigate the mechanisms which maintain the mean salinity structure of the low-latitude Pacific Ocean, and which may influence its variability on annual to decadal timescales. We use the strategy of deliberately eliminating the surface freshwater exchange in a coupled ocean–atmosphere GCM, and studying the subsequent ocean thermohaline adjustment. It is important to appreciate that this is not intended to simulate a realistic event; rather it is a sensitivity experiment designed to allow a clear identification of the key mechanisms and processes that govern the more general aspects of variability and change. If the removal of a process is observed to cause an adjustment in the system, then we may infer that the function of the process is to prevent the observed adjustment from occurring. In this sense, we are exploiting the fact that GCMs are very flexible scientific tools, allowing the simulation of experiments which could never be carried out in the real climate system.

The low-latitude Pacific is the region in which the atmosphere and ocean are most strongly coupled, and is the location of the El Niño/Southern Oscillation (ENSO), the dominant mode of interannual climate variability on the planet. Though ENSO is a thermally-dominated phenomenon—the relative roles of heat and freshwater forcing have been investigated by Schneider and Barnett (1995)—it is a vital concern to understand if (and how) it will respond to an accelerated hydrological cycle. Vialard et al. (2002) have investigated this question by performing idealized experiments using an ocean GCM with homogeneous salinity. They found that, although the mean state of the near-surface ocean was only weakly modified by removing the effects of salinity, the variability was substantially changed. This is in accord with the fact that the local salt content of the ocean is able to vary much more than the local heat content, due to the lack of rapid salinity feedbacks noted above and discussed by Pardaens et al. (2003). Furthermore, Maes et al. (2002) have reported that the salinity barrier layer (i.e. the salinity stratification in the upper layer of the western equatorial Pacific warm pool, Vialard and Delecluse 1998a, b) may affect the onset of El Niño in a coupled ocean–atmosphere GCM. This is the case because the barrier layer influences the build-up of heat in the warm pool (Maes et al. 2005). Fedorov et al. (2004) have shown that a freshening of the high-latitude surface waters, because of the melting of ice or intensification of the global hydrological cycle, may result in a transition to a permanent warm state that prevents El Niño events from occurring.

Furthermore, the focus of this paper is restricted to the *thermodynamic bowl* (Guilyardi et al. 2001), which is the part of the upper ocean that is ventilated by contact with the atmosphere on annual timescales. The thermodynamic bowl exchanges heat and freshwater with the deeper ocean, which stores the climate signals and eventually returns them to the surface. For most of the global ocean, the general agreement is that the thermodynamic bowl consists of, at most, the upper 1,000 m, corresponding to the deepest point reached by the mixed layer during the course of a year (Guilyardi et al. 2001).

This paper therefore aims to investigate the processes that maintain the salinity structure of the upper 1,000 m of the Pacific Ocean, between 40°N and 40°S, and to document the associated time scales, up to 100 years. The layout is as follows. The components of the coupled ocean–atmosphere GCM, and the coupling strategy, are described in Sect. 2, together with details of the experiments performed. The impacts on the mean thermohaline state, which include a spin-down of the haline structure and an increase in surface temperature, are analysed in detail in Sect. 3. Then, the impacts on the inter-annual variability (ENSO) are described briefly in Sect. 4. Finally, we summarize the key findings of our study in Sect. 5, and we speculate about their relevance to the response of the climate system to a future intensified freshwater cycle.

2 The experimental set-up

2.1 The coupled ocean–atmosphere general circulation model

For the present experiments, we use the *Scale INTeractions EXperiment* (SINTEX) coupled ocean–atmosphere GCM (Gualdi et al. 2003a). It is important that a coupled model is used; an ocean-only model would require prescribed surface fluxes which could bias the simulation, whereas in a coupled model these fluxes can respond dynamically to the ocean–atmosphere state. The key features of the ocean model, atmosphere model and coupler are now briefly discussed.

2.1.1 The ocean GCM

The ocean component of SINTEX is ORCA2, the global configuration of the *Océan Parallélisé* (OPA) ocean GCM developed at the *Laboratoire d'Océanographie et de Climat par Expérimentation et Approche Numérique* in Paris. A full description is given by Madec et al. (1998). The model uses a finite-difference scheme to integrate the primitive equations, using the non-linear equation of state of Jackett and McDougall (1995). A horizontal curvilinear mesh is used to overcome the North Pole singularity that arises with geographical meshes. The northern point of convergence is replaced by two poles located on Asia and North America, using the semi-analytical method proposed by Murray (1996) and implemented by Madec and Imbard (1996). The horizontal grid has 182 points in longitude (corresponding to

a resolution of 2.0°) and 149 points in latitude (corresponding to a resolution which varies from 0.5° at the equator to 2.0° at the poles). Thirty-one vertical levels are used, with ten levels in the top 100 m.

The model configuration used in the present study has a rigid lid, so that surface freshwater exchange with the atmosphere does not lead to changes in the volume of water columns. The lateral mixing of momentum is Laplacian, with a coefficient that varies from 40,000 $m^2\ s^{-1}$ at high latitudes to 2,000 $m^2\ s^{-1}$ at the equator. The lateral mixing of temperature and salinity is quasi-pure isopycnal, which prevents the development of grid-point noise so that no artificial horizontal diffusion has to be added in order to guarantee numerical stability (Guilyardi et al. 2001); the mixing coefficient is 2,000 $m^2\ s^{-1}$.

ORCA2 has been used in uncoupled mode for studies of the tropical Pacific, where Vialard et al. (2001) have shown that its climatology is in close agreement with observations (see also Delecluse and Madec 1999, and references therein). It has been used in coupled mode for process studies (e.g., Guilyardi and Madec 1997; Guilyardi et al. 2003; Gualdi et al. 2003b), palaeoclimate simulations (e.g. Braconnot et al. 1999) and climate change experiments (e.g. Barthelet et al. 1998; Dufresne et al. 2002).

2.1.2 *The atmosphere GCM*

The atmosphere component of SINTEX is ECHAM4, the GCM developed at the *Max-Planck-Institut für Meteorologie* in Hamburg. The primitive equations are solved using a spectral transform method on a T106L19 grid. The non-linear terms and physical processes are computed on a Gaussian grid with a resolution of around 1° at the equator. The model and its climatology are described in detail by Roeckner et al. (1996). We justify the use of such a high-resolution atmosphere model by noting that, when an assessment is made of the performance of several coupled GCMs each composed of different atmosphere models but of the same ocean model, the resolution of the atmosphere model appears to play an important role in correctly capturing tropical Pacific dynamics (Guilyardi et al. 2004).

2.1.3 *The coupled configuration*

In SINTEX, the ocean and atmosphere GCMs are coupled using the *Ocean Atmosphere Sea Ice Soil* coupler, OASIS2.4, developed at the *Centre Européen de Recherche et Formation Avancée en Calcul Scientifique* in France (Valcke et al. 2000). The coupling strategy is described by Guilyardi et al. (2003). Fluxes between the atmosphere and ocean are exchanged once every 2 h. There is no interactive sea ice model in the configuration used for the present experiments, since we wish to study the direct impacts of the disabled freshwater forcing, rather than any indirect impacts caused by modified high-latitude processes. Therefore, sea ice is relaxed towards an observed monthly climatology using a heat flux damping term, which tends to melt sea ice present in the model but not in the climatology, and to create sea ice present in the climatology but not in the model. Apart from this, no flux correction is applied.

2.2 The present numerical experiments

We compare two 100-year integrations of the SINTEX coupled model, both initiated from an ocean with the thermohaline structure of Levitus (1982). The oceans spin up from rest through geostrophic adjustment within a few days. In the perturbation simulation, hereafter referred to as EPR0, the net freshwater flux into the ocean (with contributions from Evaporation, Precipitation, Run-off, and formation and melting of sea-ice) is prescribed to be zero at each ocean gridpoint and each timestep. This is implemented in such a way that precipitation leads to a loss of moisture from the atmosphere but no corresponding gain by the ocean, and that evaporation leads to a gain of moisture by the atmosphere but no corresponding loss from the ocean. The latent heat flux is retained, since we do not wish to modify the thermal forcing. Similar numerical experiments have recently been performed by D. Swingedouw et al. (2006, submitted) in a sensitivity study of the Atlantic thermohaline circulation. EPR0 is compared with a full-physics control simulation, hereafter referred to as CTRL, which has interactive freshwater exchange and climatological monthly-mean river run-off. The atmospheric greenhouse gas concentrations are constant in both runs. Referring to Fig. 1, this experiment is therefore designed to investigate the route from *hydrological cycle* to *climate*, rather than the route from *climate* to *hydrological cycle*.

Before proceeding, we briefly assess the impacts of the modified freshwater forcing on the thermal and wind forcing. Figure 2 shows maps of the net heat exchange and wind stress at the ocean–atmosphere interface during the final model decade in CTRL and EPR0. The heat flux is only slightly changed between the two runs; averaged over the domain shown in the figure (40°N–40°S and 110°E–70°W) and over all 100 model years, the net downward heat flux is 6.75 W m^{-2} in CTRL and 6.79 W m^{-2} in EPR0. The wind stress forcing is also only slightly changed, meaning that the wind-driven gyre circulation is barely affected by the disabled freshwater forcing. Therefore the changes described in the remainder of this paper may all be interpreted as direct responses to the modified freshwater flux, rather than indirect responses to a modified momentum or heat flux caused by the modified freshwater flux. In the following sections, we analyse the adjustment of the decadal mean (Sect. 3) and interannual variability (Sect. 4) of the thermohaline structure of EPR0 relative to CTRL.

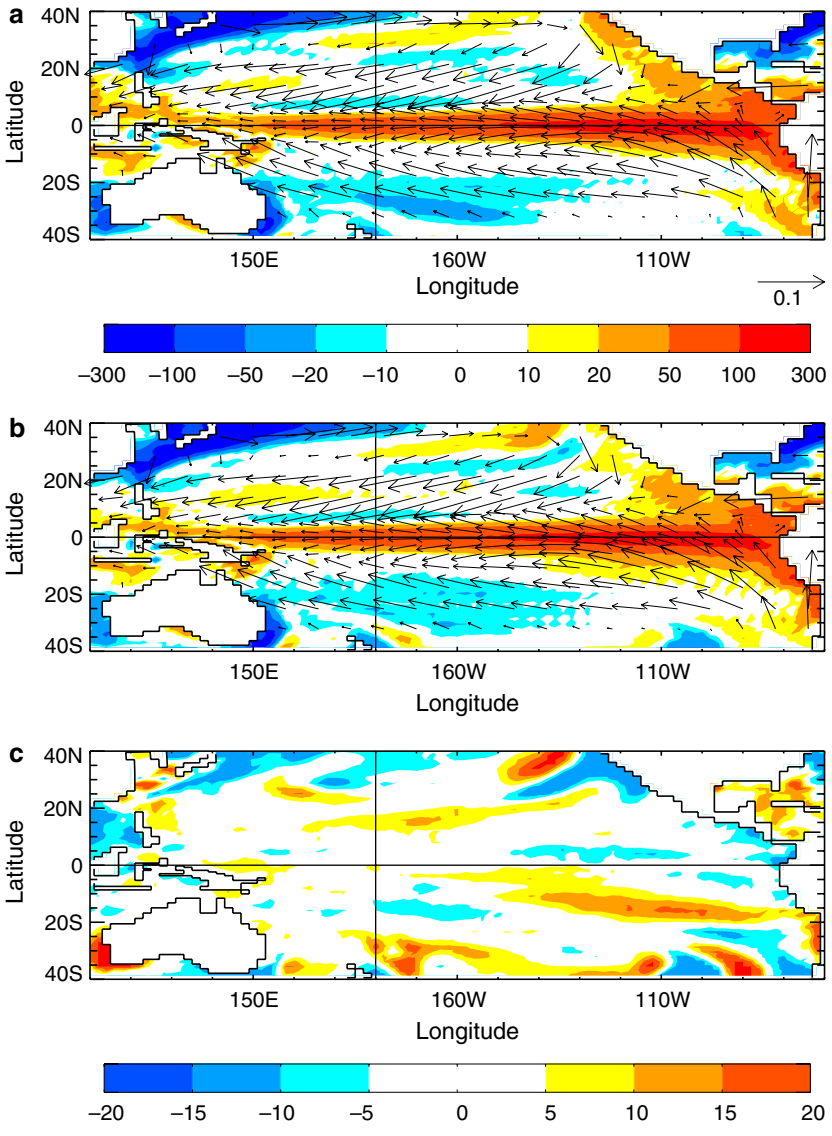

Fig. 2 Maps of net downward surface heat flux (W m^{-2}, *contours*) and surface wind stress (N m^{-2}, *vectors*) in the Pacific, averaged over model years 91–100, **a** in CTRL, and **b** in EPR0. The difference (W m^{-2}) between the net downward surface heat fluxes in **b** and **a** is shown in **c**

3 Impacts on the decadal-mean state

3.1 Salinity structures and their relation to freshwater forcing

The global decadal-mean net surface freshwater forcing over the ocean in the fourth decade of CTRL is shown in Fig. 3a; the corresponding plot for EPR0 is not shown, since it is zero everywhere. The key features in the figure may be understood by noting that evaporation is expected to be strong at low latitudes, where the surface is warm and windy. Precipitation is low over the subtropical gyres in the Pacific, Indian and Atlantic oceans (between around 10–30°N and 10–30°S), which are regions of horizontally-diverging surface atmospheric flow and vertical descent. Precipitation is high over the Inter-Tropical Convergence Zone (ITCZ, centred at around 10°N in the Pacific), the South Pacific Convergence Zone (SPCZ, centred at around 10°S), the northern subpolar gyres in the Pacific and Atlantic oceans (between around 40 and 60°N) and in the Southern ocean (between around 50 and 70°S), all of which are regions of horizontally-converging surface atmospheric flow and vertical ascent. The tendency of the SINTEX model to produce something more like a double ITCZ, rather than a true SPCZ inclined at an angle to the equator as observed, has been noted by Gualdi et al. (2003a) and is a common systematic error of coupled GCMs. Run-off of freshwater from rivers is present in Fig. 3a as localized downward contributions to the flux at the boundaries with the continents.

The decadal-mean sea surface salinity (SSS) in CTRL, resulting from the freshwater forcing in Fig. 3a, is shown in Fig. 3b. In general, regions of high (low) SSS are strongly correlated with regions of net upward (downward) freshwater flux. In common with most coupled GCMs used for climate simulation, the western equatorial Pacific is marked by unrealistically high

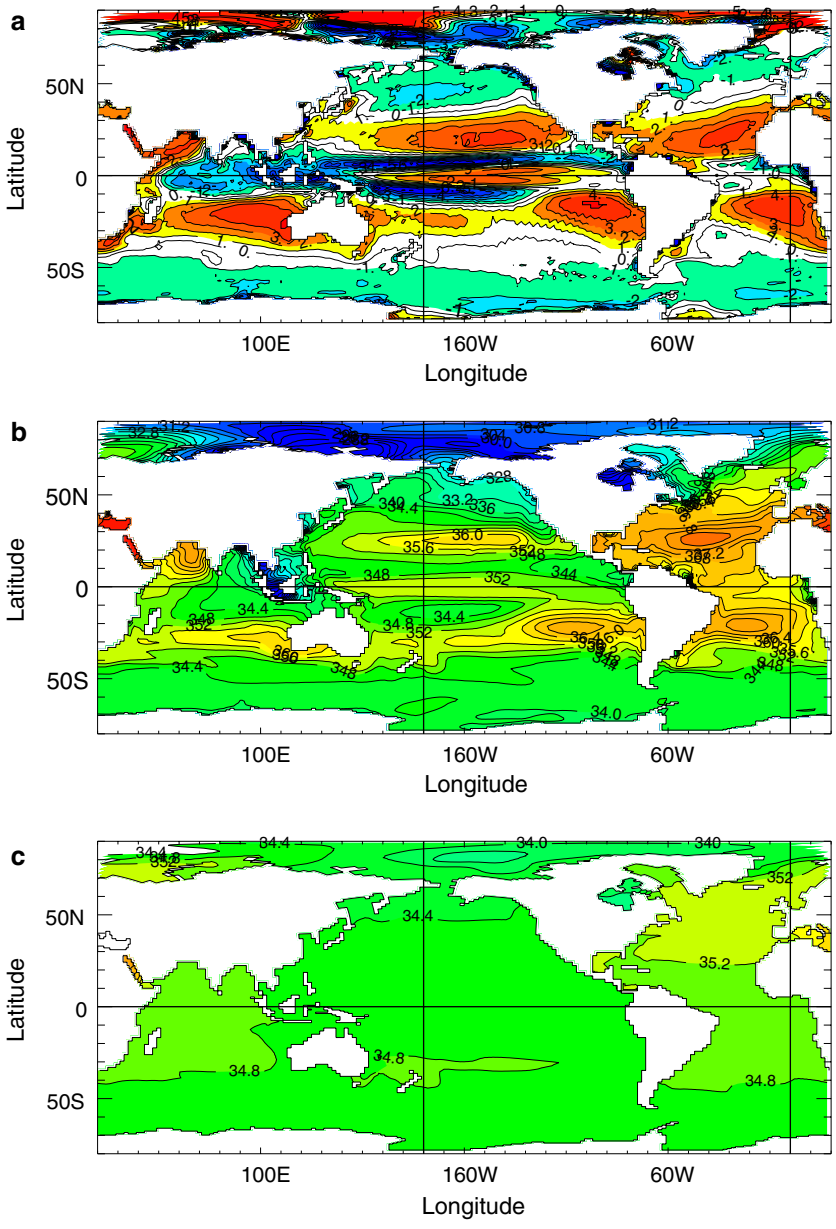

Fig. 3 Global maps of **a** net upward surface freshwater flux (mm day^{-1}) in CTRL, **b** sea surface salinity (psu) in CTRL, and **c** sea surface salinity (psu) in EPR0. An average is taken over model years 31–40 in all three maps

salinity due to the penetration of the equatorial cold tongue too far to the west. However, although the mean tropical salinity distribution departs from observations, the broad features and basic structures are present. Excluding the Mediterranean and Red Seas, the SSS in the plot ranges from 26.7 psu in Hudson Bay to 38.3 psu in the north Atlantic subtropical gyre. For comparison, the corresponding decadal-mean SSS in the fourth decade of EPR0 is shown in Fig. 3c. Strikingly, all of the surface salinity structures present in CTRL have been severely eroded. Again excluding the Mediterranean and Red Seas, the SSS ranges only from 33.5 psu in Hudson Bay to 35.4 psu in the north Atlantic. The decay processes are noticeably quicker in the tropics than at high-latitudes. They are also quicker in the Pacific than in the Atlantic and Indian oceans, due to the existence of deep structures connected to the surface in the north Atlantic giving access to a longer-term memory, and also to the outflow of saline waters from the Mediterranean and Red Seas. The surface salinity homogenization continues throughout the model integration, although most of it is achieved by the fourth decade.

Figure 4 shows the vertical and meridional structure of zonally-averaged salinity in the Pacific Ocean. In the initial conditions (Fig. 4a), the fresh, shallow signatures of the ITCZ and, to a lesser extent, the SPCZ, are visible as surface salinity minima near 10°N and 5°S. The signatures of the subtropical gyres, which are visible as subsurface salinity maxima near 25°N and 15°S, penetrate to greater depths. In CTRL, both of these salinity maxima rise to the surface at certain longitudes and times of the year. The fresh signal of the northern subpolar

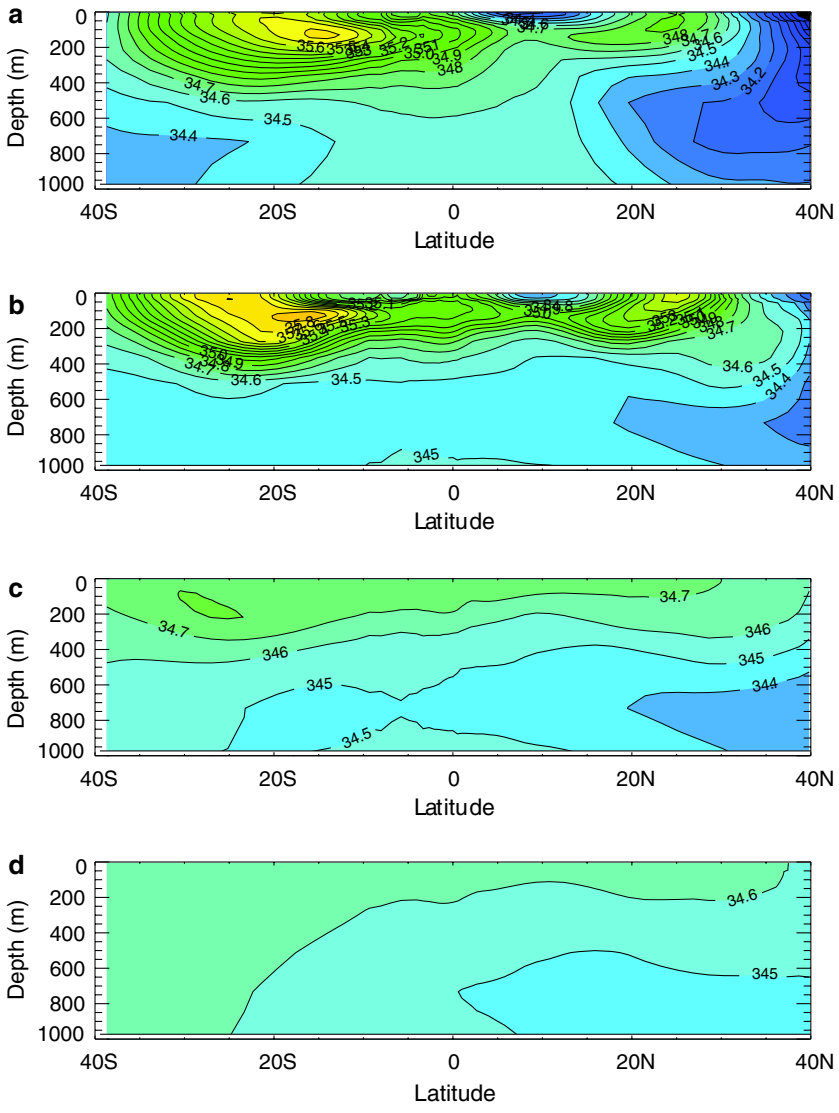

Fig. 4 Depth–latitude plots of zonal-mean salinity (psu) in the top 1,000 m of the Pacific Ocean, **a** in the Levitus (1982) initial conditions, **b** in CTRL averaged over model years 31–40, **c** in EPR0 averaged over model years 31–40, and **d** in EPR0 averaged over model years 91–100. The zonal average is taken over longitudes 110°E–70°W in all four cases

gyre, at around 40°N, penetrates deeper still, and corresponds to the formation of North Pacific Intermediate Water (NPIW). The fresh signal of the Southern Ocean, south of 40°S, penetrates to similar depths, and corresponds to the formation of Antarctic Intermediate Water (AAIW). The north–south asymmetry present in Fig. 4a is a consequence of the asymmetrical surface freshwater forcing: the ITCZ is displaced north of the equator and there is no subpolar gyre in the south Pacific.

The same broad features and basic structures are present in the fourth decade of CTRL (Fig. 4b). In contrast, by the fourth decade of EPR0 (Fig. 4c), the ITCZ and SPCZ signals are no longer present. The southern subtropical gyre subsurface salinity maximum has been reduced from 35.8 to 34.8 psu, and has drifted southward by 10–15° of latitude. Due to the surface salinity changes in the AAIW formation region, the southern hemisphere salinity minimum with respect to depth, caused by the equatorward propagation of AAIW, disappears completely by the final decade (Fig. 4d). Similarly, the northern hemisphere salinity minimum due to the equatorward propagation of NPIW is greatly weakened. The same qualitative features in zonal-mean salinity are seen in the Atlantic and Indian oceans in EPR0. We quantify the time scale of the salinity homogenization in Sect. 3.3.

3.2 Impacts on temperature, mixed-layer depth and density

Figure 5a shows how the annual-mean Pacific-averaged SST changes with time in both simulations. It is seen that the SST in CTRL drifts from the common initial value during the first decade (although the adjustment to the observed initial conditions is small for a non-flux-adjusted coupled GCM), and that EPR0 warms relative to CTRL by 0.6°C by the final decade. The relative warming occurs on a decadal timescale, and most of it is achieved by the end of the third decade. Time series of

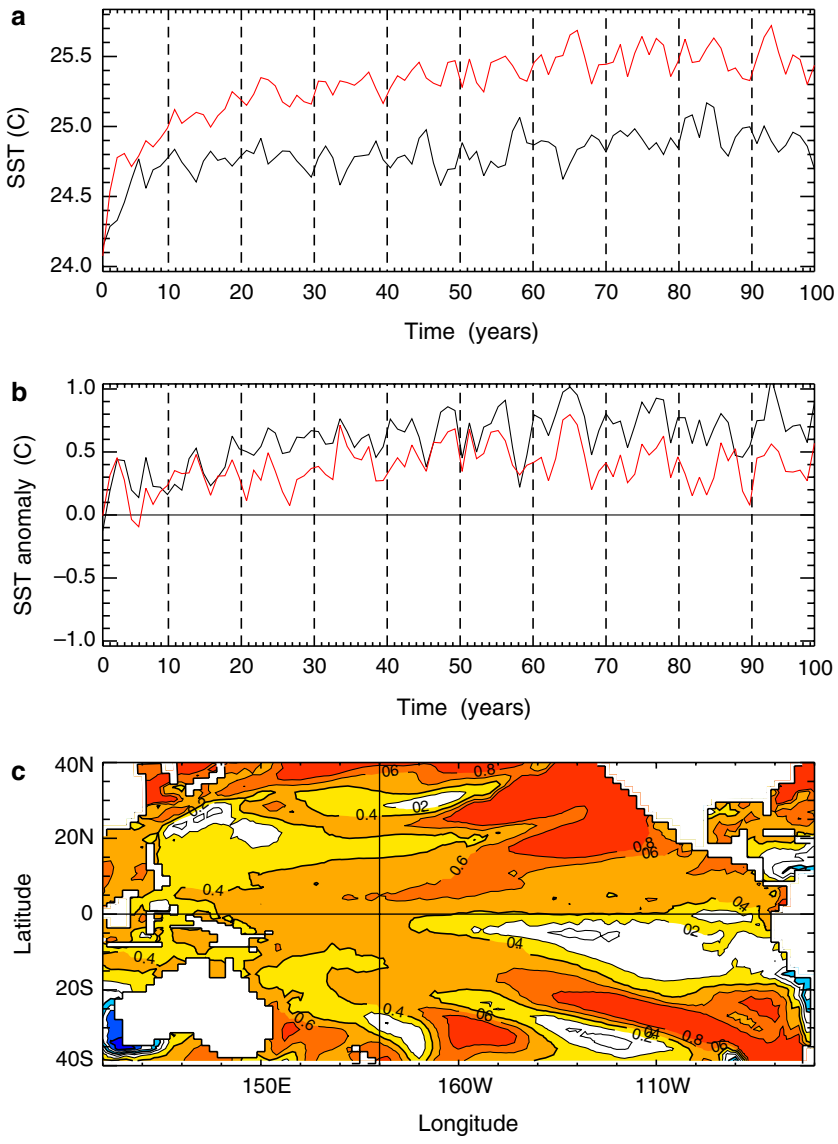

Fig. 5 **a** Time series of annual-mean Pacific sea surface temperature in CTRL (*black curve*) and EPR0 (*red curve*). The averaging domain is 40°N–40°S and 110°E–70°W. **b** Time series of annual-mean Pacific sea surface temperature anomaly (EPR0–CTRL) averaged over the northern (*black curve*) and southern (*red curve*) halves of the domain used in **a**. **c** Map of Pacific sea surface temperature anomaly (EPR0–CTRL, °C) averaged over model years 31–40

the anomalous (EPR0–CTRL) surface warming are shown in Fig. 5b, with the north and the south of the equator treated separately. The warming relative to the control is meridionally asymmetrical, reaching 0.7 and 0.4°C north and south of the equator, respectively, when averaged over the final 50 years. This asymmetry will be explained in terms of the freshwater flux asymmetry in Sect. 3.3.5. The spatial pattern of the SST anomaly achieved by the fourth decade is shown in Fig. 5c. A decadal mean is taken, in order to average over the inter-annual (ENSO-related) variability seen in Fig. 5a, b. The north–south asymmetry noted above is clearly visible, and the relative warming is seen to reach around 1.0°C locally. The mechanism responsible for the decadal thermal adjustment will be identified in Sect. 3.3. We note here that the mechanism appears to be important only in EPR0, since the SST in CTRL appears to reach a new statistical equilibrium by year 5, with no apparent subsequent decadal trend (Fig. 5a).

Figure 6a, b shows the freshwater forcing (CTRL) and mixed-layer depth anomaly (EPR0–CTRL), both zonally averaged in the Pacific. Here, the bottom of the mixed layer is computed as the depth at which the density exceeds the local surface density by 0.01 kg m^{-3}. The two curves in the mixed-layer depth plot are averages over the first year and the first decade. They correspond reasonably well, demonstrating that the mixed-layer adjustment is very rapid (within 1 year). We have looked at annual-mean zonal-mean mixed-layer depth anomalies in each of the first 10 years; whilst there is appreciable inter-annual variability, each of the annual means displays the same broad features as seen in the decadal mean in the figure. The correspondence at low latitudes (between 15°N and 15°S) is better than at higher latitudes, because the higher latitudes are influenced by subtropical gyres which operate on slower, decadal timescales. Under the ITCZ (5–10°N) and SPCZ (5–10°S), which are both regions of net precipitation in CTRL (Fig. 6a), there is a

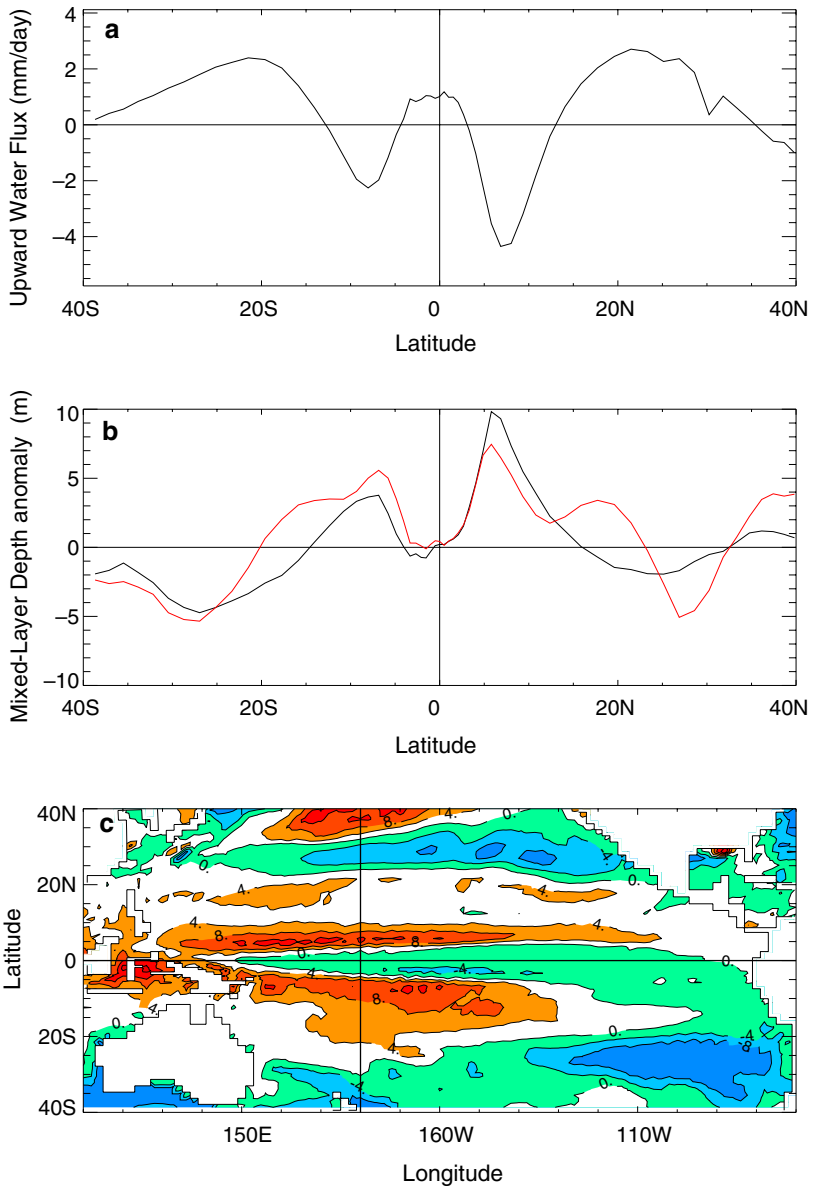

Fig. 6 **a** Net upward surface freshwater flux in CTRL, zonally averaged in the Pacific between 110°E and 70°W over model years 1 and 10. **b** Mixed-layer depth anomalies (EPR0–CTRL), zonally averaged in the Pacific between 110°E and 70°W over model years 1 (*black*) and 1–10 (*red*). **c** Map of the mixed-layer depth anomaly (EPR0–CTRL, m) in the Pacific, averaged over model years 1–10

deepening of the mixed layer in EPR0 (Fig. 6b). This occurs because, when the freshwater forcing is disabled, there is a rapid surface salinity increase at these latitudes, giving denser surface waters and enhanced vertical mixing. Conversely, within the subtropical gyres (15–35°N and 15–40°S), which are both regions of net evaporation in CTRL, there is a shallowing of the mixed layer in EPR0. This occurs because, when the freshwater forcing is disabled, there is a rapid surface salinity decrease at these latitudes, giving more buoyant surface waters and inhibited vertical mixing.

The correspondence between mixed-layer depth changes and control freshwater flux is further confirmed by comparing the first-decade mixed-layer depth anomaly map in Fig. 6c with the CTRL freshwater flux map in Fig. 3a. The spatial correlation between the two maps, computed within the latitude and longitude ranges 40°N–40°S and 110°E–70°W, is −0.62. The correspondence between mixed-layer depth anomaly and SST anomaly (Fig. 5c) is poor, however, suggesting that the decadal warming trend is driven not by changes in the mixed layer (which operates on much faster timescales) but by changes in the deeper ocean. We note that Deser et al. (1996) report mixed-layer depth changes accompanying SST changes in observations of the north Pacific and, as in our study, the spatial distributions of the two are different.

Figure 7 shows the evolution of vertical profiles of anomalous salinity, temperature and potential density, averaged in the Pacific. In CTRL, evaporation exceeds precipitation plus run-off by 0.6 mm day^{-1} when averaged over the domain under consideration (40°N–40°S and 110°E–70°W), and so there is a relative freshening of the surface in EPR0 (Fig. 7a). The freshening is by a

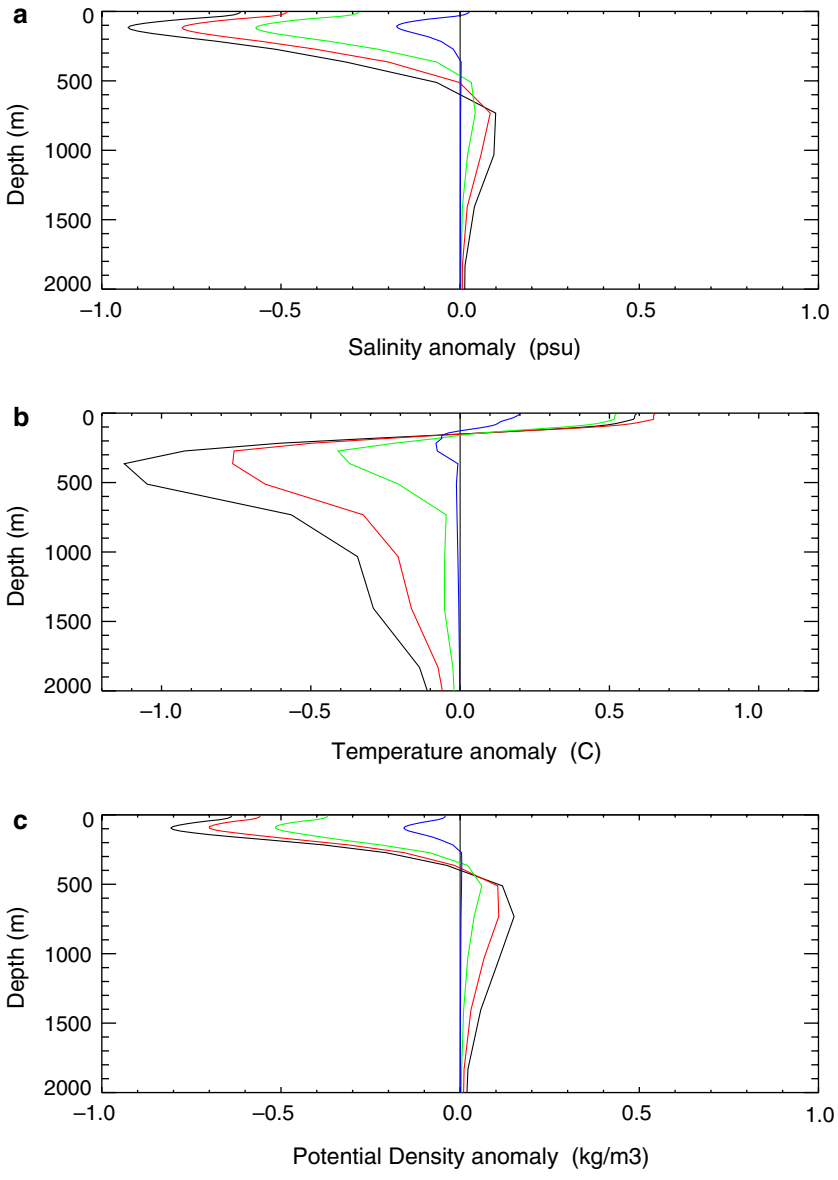

Fig. 7 Vertical profiles of Pacific anomalies (EPR0–CTRL) of **a** salinity, **b** temperature, and **c** potential density. The averaging domain is 40°N–40°S and 110°E–70°W. The averaging period is model years 1–10 (*blue curves*), years 31–40 (*green curves*), years 61–70 (*red curves*) and years 91–100 (*black curves*)

maximum value of 0.9 psu and extends down to around 500 m by the end of the run. Beneath this, there is a weak salinity increase (up to around 0.1 psu). The rate of anomalous near-surface freshening, $-\mathrm{d}\bar{S}/\mathrm{d}t$, averaged over this horizontal domain and over depth d of the upper ocean, is consistent with a simple calculation based on the mean CTRL freshwater flux, $E - P - R$, which predicts

$$-\frac{\mathrm{d}\bar{S}}{\mathrm{d}t} = \frac{\bar{S}(E-P-R)}{d}. \quad (1)$$

Using a mean salinity of $\bar{S} = 35\,\mathrm{psu}$, $E - P - R = 0.6\,\mathrm{mm\,day^{-1}} = 22\,\mathrm{m\,century^{-1}}$ and $d = 500\,\mathrm{m}$, gives $-\mathrm{d}\bar{S}/\mathrm{d}t = 1.5\,\mathrm{psu\,century^{-1}}$. This is slightly larger than (although the same order of magnitude as) the upper-ocean freshening seen in Fig. 7a, suggesting that there may also be an anomalous net meridional transport of salt, not captured by this calculation.

The relative surface warming in EPR0, which reaches a maximum value of around 0.6°C as previously noted, is seen in Fig. 7b to be confined to the upper 200 m. Below this there is a relative cooling, whose maximum value increases and gradually deepens with time, reaching 1.1°C at around 350 m by the final decade. The effects of surface warming and freshening together cause the near-surface density to decrease by up to 0.8 kg $\mathrm{m^{-3}}$ by the end of the integration, and there is an increase in the density below 400 m by up to 0.15 kg $\mathrm{m^{-3}}$ (Fig. 7c). By decomposing the potential density anomaly into a thermal and a haline contribution, using a linearized equation of state, we find that the two contributions are roughly equal, with the haline contribution exceeding the thermal contribution by a factor which reaches a maximum value of around 2 in the surface layers (not shown). This contrasts with the usual dominance of thermal effects over haline effects in the tropics, but is

not surprising given the large freshwater perturbation applied.

3.3 Mechanism for the decadal thermal adjustment

The vertical profiles of temperature anomaly shown in Fig. 7b suggest that the decadal SST increase in EPR0 relative to CTRL is caused by a net transfer of heat from those waters below 200 m to the surface layers. We now present evidence, first qualitative (Sect. 3.3.1) and then quantitative (Sects. 3.3.2, 3.3.3), that the physical mechanism responsible for this thermal adjustment is a change in the along-isopycnal diffusive heat flux.

3.3.1 Qualitative heat budget

Consider the heat balance of the upper 200 m of the Pacific Ocean (corresponding to the layer that warms), between the nominal latitudes of 40°N and 40°S. The terms in the heat budget equation for this box are as follows. Averaged over the upper boundary, the ocean takes up heat from the atmosphere (Fig. 2, Sect. 2.2). At the northern and southern boundaries, isopycnal advection due to the basin-scale gyre circulations exports heat from the box. At the lower (200 m) boundary, equatorial upwelling imports heat into the box. In addition, isopycnal mixing of waters of different temperatures causes a heat flux with a mainly horizontal, but also a smaller vertical, component. Lastly, diapycnal mixing of waters of different temperatures causes a heat flux with a mainly vertical (downward), but also a smaller horizontal, component. An approximate balance between all these contributions to the heat budget exists in CTRL.

Let us now consider, qualitatively, how each of these contributions changes in response to the modified freshwater forcing in EPR0. The equilibrium mean heat flux into the ocean across the upper surface increases by 0.04 W m^{-2} between the two experiments (Sect. 2.2). This change will shortly be shown to be too small to cause the observed SST increase, and furthermore, any increase in this term could not explain the cooling at depth. The vertical velocity of the wind-driven upwelling is unchanged, since the surface wind stress is unchanged (Fig. 2), and so it seems unlikely that the upwelling heat flux at the lower boundary is the cause of the thermal changes (although this flux may adjust in response to the modified vertical temperature gradients, once they are established via another mechanism). We note that the 200 m surface lies within the thermocline, a region of strong stable statification and minimum vertical diffusivity that is unchanged in EPR0. The gyres do not appreciably accelerate or decelerate between the two experiments (Sect. 2.2), and so the changes in meridional velocity at the northern and southern boundaries are small. Changes to the meridional temperature gradients are also small: the change at the surface on the equator at the dateline is from 0.271°C per degree of latitude in CTRL to 0.277°C per degree of latitude in EPR0. Therefore changes in the net advective heat flux are small, and anyway cannot explain the vertical structure of the temperature anomalies, and so can immediately be ruled out as the cause of the observed thermal changes. The remaining term in the heat budget equation—the heat flux due to isopycnal mixing—is the term which changes by far the most, in percentage terms, in response to the disabling of the surface freshwater flux. In fact, this term tends to zero in EPR0, as we discuss next. A change to the vertical component of this flux therefore appears to be a good candidate to explain the observed vertical heat transfer.

To understand how isopycnal mixing causes an along-isopycnal heat flux in the real ocean and in CTRL, consider the schematic diagram of Fig. 8. Isopycnal surfaces (i.e. surfaces of constant density) are surfaces of greatly-enhanced ocean mixing. The existence of isopycnal salinity gradients (e.g. Fig. 10), which are forced ultimately by the spatial pattern of the surface freshwater flux and ventilation processes, implies the existence of density-compensating temperature gradients (the origins and physics of which have been studied recently by Yeager and Large 2004; Tailleux et al. 2005). Isopycnal mixing therefore causes an along-isopycnal heat transfer, in the direction from warm to cold anomalies, and ultimately between the atmosphere and the deep ocean where the climate signal is stored (Guilyardi et al. 2001). Salinity plays a crucial role in this heat transfer, since it is only in the presence of an inhomogeneous salinity field that isopycnal surfaces are inclined at an angle to isothermal surfaces.

As salinity becomes homogeneous in EPR0 (Fig. 4), isopycnal surfaces begin to coincide with isothermal surfaces, and the along-isopycnal salinity gradients are therefore eroded. The density-compensating along-isopycnal temperature gradients must also be eroded, causing the heat flux due to isopycnal mixing to tend to zero. As suggested by Fig. 8, the *vertical* component of this heat flux at low latitudes is directed downwards, both in our model (see Sect. 3.3.2) and in the real ocean (Osborn 1998). Therefore it is the gradual shutdown of this term in the heat balance equation, with the other terms remaining approximately unaltered as discussed above, that appears to lead to the net upward transfer of

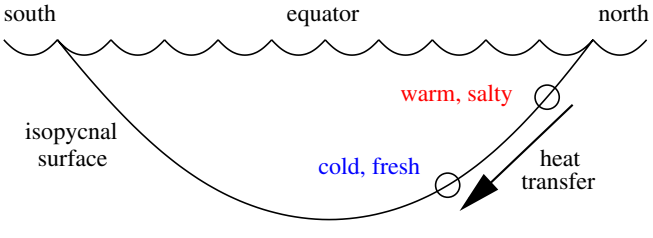

Fig. 8 Schematic diagram to show how isopycnal mixing in the presence of density-compensating temperature and salinity gradients results in an along-isopycnal heat transfer

heat seen in EPR0. The result is an initial transfer of heat from the interior to the surface. Presumably a new equilibrium is reached when the upwelling heat flux is reduced (due to the cooling at depth) to the point at which it is balanced by the downward diapycnal diffusive heat flux. Furthermore, the gradual shutdown in EPR0 of the *meridional* component of the along-isopycnal heat flux at 40°N and 40°S (which is directed equatorward in CTRL) is consistent with the net cooling of the box seen in the temperature profiles of Fig. 7b.

It is interesting to note that a similar net vertical heat transfer to that described above was observed during the development of HadCEM (Roberts et al. 2004). A surface cooling was obtained during the tuning of the model. This was found to be due to the advection scheme, which was initially a third-order scheme and hence more diffusive than the second-order scheme used in HadCM3. This extra diffusion had the effect of moving heat downwards from the surface to the interior. The advection scheme had to be changed to a fourth-order scheme, which was much less diffusive and improved the SSTs (M.J. Roberts, personal communication). In our experiments, too, the SST is modified by changing the mixing characteristics, although in our case the change is physical rather than numerical.

Having identified the mechanism believed to be responsible for the thermal adjustment in EPR0, we next check that the amplitude (Sect. 3.3.2) and timescale (Sect. 3.3.3) of the SST increase predicted by the mechanism are consistent with those seen in the model (i.e. a surface warming of 0.6°C within a few decades).

3.3.2 *Amplitude of the thermal adjustment*

In order to estimate the anomalous surface warming expected in EPR0 according to the conjectured mechanism, we need control values of the vertical component of the along-isopycnal diffusive heat flux. Since this is not a standard diagnostic produced by our model, we ran a separate 10-year ocean-only simulation in which the flux is computed and output. The prescribed surface heat and momentum fluxes for the run are taken from the ERA-40 climatology (Uppala et al. 2005) averaged over the period 1979–1988, and are applied daily. The SST is relaxed back to the Reynolds (1988) climatology from the same period, with a strength of 40 W m^{-2} K^{-1}. The simulation is initiated from an ocean at rest with the thermohaline structure of Levitus (1982).

Figure 9 shows a vertical profile of the flux so obtained in the low-latitude Pacific Ocean, averaged over the tenth year of the forced simulation. The flux is directed downwards and is small below 1,000 m, but reaches a peak of around 4 W m^{-2} near 200 m. This peak coincides with the zeros of the temperature anomalies in Fig. 7b, as it must do if the hypothesized mechanism is indeed responsible for the thermal adjustment. The mean value of the flux is around $Q = 1$ W m^{-2}. Both in sign and magnitude, this is consistent with the estimate of Osborn (1998), who used observations of the time-mean thermohaline state of the world oceans for his computation. This consistency indicates that the isopycnal diffusive heat flux mechanism in our model resembles that which is inferred for the real ocean.

An estimate of the size of the anomalous near-surface warming, ΔT, expected to result from the shut-down of this heat flux in EPR0, averaged over depth d of the upper ocean, at time t after the model integrations start, is given by a simple calculation to be

$$\Delta T = \frac{Qt}{d\rho c}, \tag{2}$$

where ρ is the mean density and c is the mean specific heat capacity. Using $Q = 1$ W m^{-2}, $t = 20$ years, $d = 200$ m, $\rho = 1{,}020$ kg m^{-3} and $c = 4{,}200$ J kg^{-1} K^{-1}, we obtain $\Delta T = 0.7$°C, in reasonable agreement with the near-surface temperature increase seen in Fig. 5a. If this calculation is repeated with Q equal to the change in the diapycnal heat flux or the change in the surface heat flux, rather than the change in the vertical component of the along-isopycnal diffusive heat flux, then the temperature change predicted is much smaller and is unable to account for the temperature change seen in the model.

3.3.3 *Timescale of the thermal adjustment*

Since the rate at which the isopycnal heat flux is shut down is determined by the rate at which salinity gradients are eroded, we now quantify the timescale of the salinity homogenization discussed in Sect. 3.1. We illustrate our method by showing, in Fig. 10, maps of annual-mean salinity in EPR0 on the isopycnal (constant potential density) surface defined by $\sigma_0 = 24.0$, which outcrops at latitudes of around 30° and reaches a

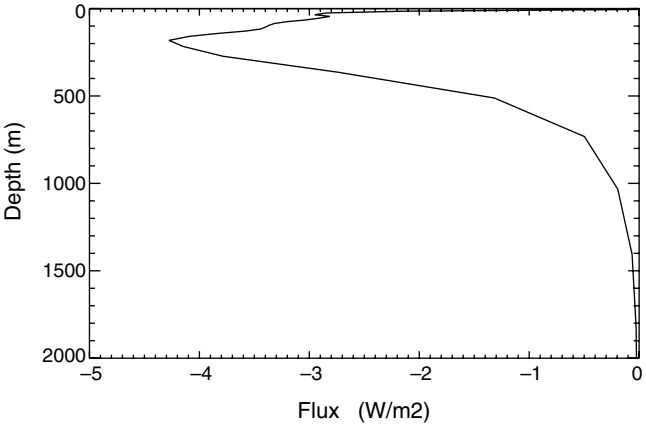

Fig. 9 Vertical component of the annual-mean along-isopycnal diffusive heat flux in an ocean-only simulation. The quantity is averaged in the low-latitude Pacific and over the tenth year of the simulation. Negative values indicate a downward flux. The latitude and longitude ranges for the averaging are 40°N–40°S and 110°E–70°W

maximum depth of around 100 m. In the first year (Fig. 10a), this isopycnal surface exhibits relatively large spatial variations in salinity, from 33.6 psu near the outcrop in the north-east Pacific to 36.2 psu near the outcrop in the south-central Pacific. As previously noted, the existence of salinity anomalies on an isopycnal surface implies the existence of density-compensating temperature anomalies, which in this case vary from 19.0 to 25.8°C (not shown). These are the anomalies responsible for the along-isopycnal heat transfer depicted in Fig. 8. As the EPR0 integration proceeds (Fig. 10b–d), the isopycnal salinity (and temperature) anomalies are eroded. We note here that our use of potential density, rather than the strictly-correct neutral density used by the model physics, is a valid approximation for these diagnostics since we are interested only in the upper 1,000 m where the two are similar.

The depth of isopycnal surfaces displays a characteristic W-shaped variation with latitude, and it is impossible to tell from Fig. 10 whether the local slope is up or down to the north. Therefore, the sign of the vertical component of the along-isopycnal heat flux is unclear from this figure alone. However, the detailed computation of Sect. 3.3.2 showed that the vertical component is directed downwards when averaged over the low-latitude Pacific Ocean.

In order to quantify the mixing processes responsible for the decaying anomalies, Fig. 11a shows time series of the spatial standard deviation of annual-mean salinity on the $\sigma_0 = 24.0$ isopycnal surface, in both simulations. There is a slight negative long-term drift in CTRL, superimposed on which is appreciable inter-annual to inter-decadal variability due to natural variations in the surface freshwater forcing. The EPR0 curve exhibits exponential decay with an *e*-folding time of 11 years, with no inter-annual to inter-decadal variability since the surface freshwater forcing does not vary on these (or any) timescales in this run. The decay of isopycnal salinity anomalies to zero in EPR0 is consistent with the assertion of Schneider and Bhatt (2000) that, in a steady state, the distribution of a tracer with no boundary fluxes or internal sources will be constant everywhere.

The exponential decay in EPR0 occurs because salinity on isopycnal surfaces is dynamically passive, and it therefore behaves like a passive tracer. Passive tracer anomalies asymptotically decay to zero exponentially for steady flow without sources or sinks, and for unsteady flow the underlying trend is still exponential (Haine and Hall 2002). The decay rate is given by the eigenvalue of the gravest eigenmode of the transport operator. For simple instances of the transport operator, the *e*-folding time of the decay, τ, depends upon the

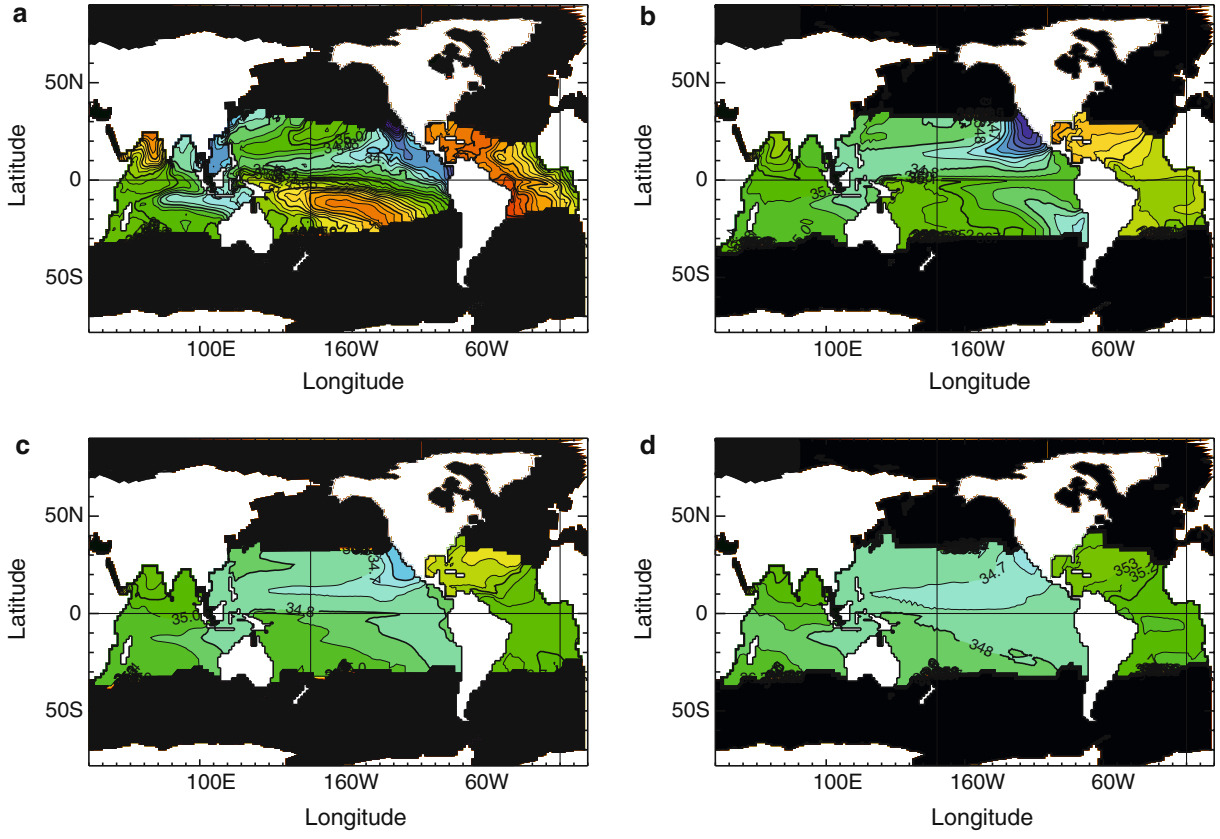

Fig. 10 Global maps of annual-mean salinity (psu) in EPR0 on the isopycnal surface defined by $\sigma_0 = 24.0$, in **a** year 1, **b** year 11, **c** year 21, and **d** year 31. *Black shading* indicates outcropping of the isopycnal surface, i.e. regions for which σ_0 is greater than 24.0 at all depths

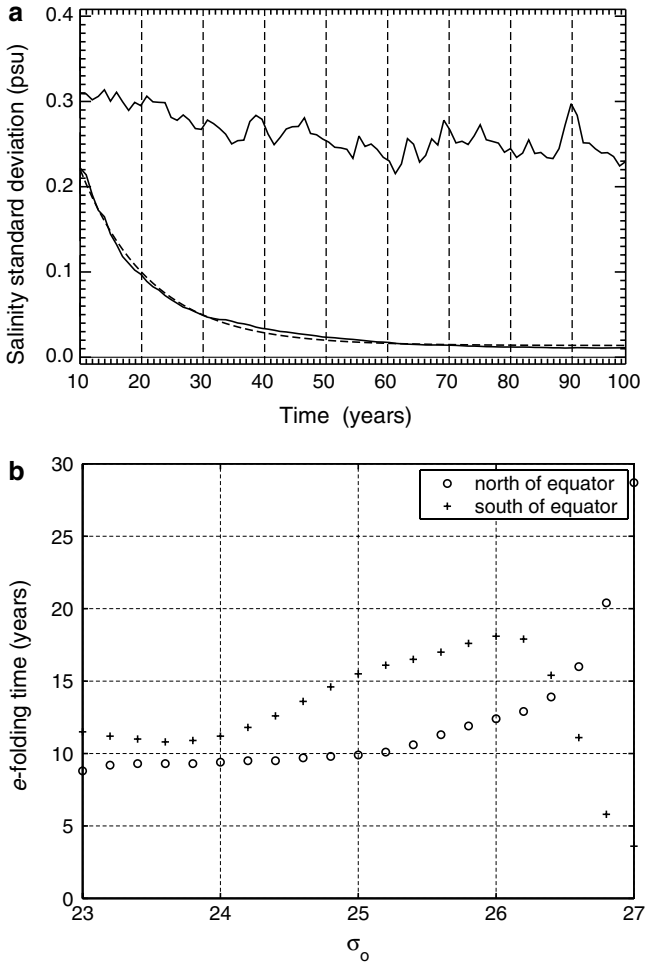

Fig. 11 **a** Time series of the spatial standard deviation of annual-mean salinity in CTRL (*upper solid line*) and EPR0 (*lower solid line*) on the isopycnal surface defined by $\sigma_0 = 24.0$. The spatial standard deviation is computed between the longitudes 110°E and 70°W, and between the latitudes of outcrop. The exponential curve of best fit for EPR0 is also shown (*dashed*), and is used to define an *e*-folding time. Model years 1–9, in which there is an adjustment to the initial conditions, are discarded for the purposes of the curve fitting. **b** *e*-folding times for the decay of the spatial standard deviation of annual-mean salinity on isopycnal surfaces in EPR0, as functions of σ_0, both north (*circle*) and south (*plus*) of the equator

characteristic length scale, L, and the isopycnal diffusivity, κ, according to $\tau = L^2/\kappa$. For more complex cases (e.g. complicated domain shape, non-uniform κ) there is no closed form solution and one cannot calculate the gravest eigenvalue, but it seems quite reasonable that $\tau = L^2/\kappa$ should still give a good estimate (T. Haine, personal communication). Noting that the present ocean model uses $\kappa = 2{,}000\ \mathrm{m^2\ s^{-1}}$, for a low-latitude anomaly spanning 10° of longitude or latitude this estimate predicts an *e*-folding time of 16 years.

The *e*-folding time for the decay of salinity gradients in EPR0 has been computed for the isopycnal surfaces defined by $\sigma_0 = 23.0, 23.2, 23.4, \ldots, 27.0$. The results of this calculation are shown in Fig. 11b, in which separate calculations are performed for the regions north and south of the equator (mindful of the north–south asymmetry of salinity structures in Fig. 4a). The *e*-folding time is generally in the range 10–20 years, in broad agreement with the estimate of the previous paragraph. The general trend of increasing *e*-folding time with increasing σ_0, seen in the figure, is due (at least in part) to the effects of increasing area, since isopycnal surfaces with higher values of σ_0 outcrop at higher latitudes, and also possibly to the effects of decreasing circulation with depth. The rapid reduction in *e*-folding time south of the equator, as the density increases above $\sigma_0 = 26.0$, appears to be associated with enhanced mixing due to the shearing influence of the Antarctic Circumpolar Current (ACC), since the $\sigma_0 = 26.0$ surface outcrops at the northern-most limit of the ACC in the Pacific Ocean (~45°S).

The timescale for the decay of salinity gradients (10–20 years) therefore matches the timescale for the vertical heat transfer (Figs. 5b, 7b). This, combined with the evidence of Sect. 3.3.2, leads us to assert that the mechanism responsible for the observed thermal adjustment in EPR0 is the shutdown, in response to the disabled freshwater forcing, of the vertical heat flux caused by isopycnal mixing.

3.3.4 Analysis using density co-ordinates

We next seek to analyse the water-mass transformations which result from disabling the surface freshwater flux. In particular, we wish to distinguish between isopycnal transformations (i.e. those which leave the density unchanged) and diapycnal transformations (i.e. those which change the density, due to contact with the atmosphere or diapycnal mixing). Once again, we employ potential density rather than neutral density.

For this purpose, it is convenient to introduce the concept of *spiciness*, which describes the temperature and salinity of water with a given density (Veronis 1972; Munk 1981). Warm and salty water has a high spiciness, and vice versa. It is often more convenient to describe water masses in terms of their density and spiciness rather than their temperature and salinity. This is because density and spiciness are process-oriented quantities: density affects ocean dynamics through its influence on internal pressure gradients, and spiciness affects the air–sea interaction (Schneider 2004). The transformation between (tempature, salinity) and (density, spiciness) co-ordinates is illustrated schematically in Fig. 12. Isopycnal water-mass transformations may now be interpreted as those which involve a change of spiciness at constant density.

Figure 13 shows the time evolution, in the (temperature, salinity) plane, of the average water-mass properties of two fixed boxes both spanning 40°N–40°S and 110°E–70°W. The depth ranges of the boxes are chosen by reference to the vertical profiles in Fig. 7: in the depth range 0–100 m, EPR0 becomes warmer, fresher and less dense relative to CTRL, and in the depth range 200–

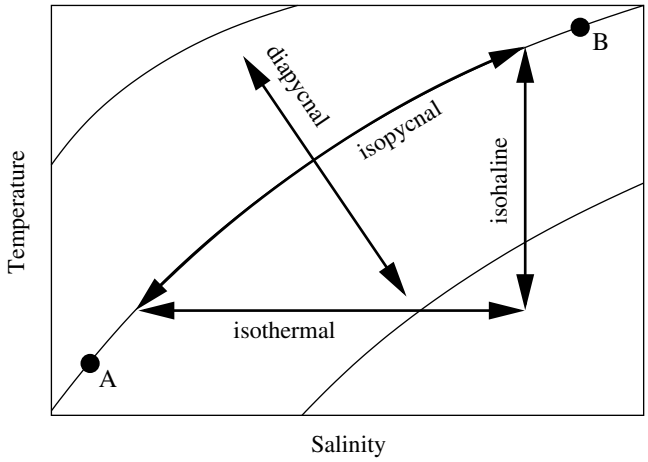

Fig. 12 Schematic illustration of the relationship between temperature, salinity, density and spiciness. The *curved lines* are contours of constant density (i.e. isopycnals), and they are curved because of non-linearities in the equation of state. Water-masses *A* and *B* have the same density, but *B* has a higher spiciness than *A*. Isothermal, isohaline and isopycnal transformations describe water-mass changes at constant temperature, salinity and density, respectively. Diapycnal transformations describe water-mass changes perpendicular to the isopycnal curves

400 m it becomes cooler, fresher and slightly less dense. In the top 100 m (Fig. 13a), CTRL and EPR0 exhibit a more-or-less common quasi-isohaline temperature increase of around 0.6°C in the first 5 years, due to initial-condition adjustment (see also Fig. 5). Subsequently, the trajectories diverge markedly. The dominant transformation in CTRL is a steady isothermal drift to higher salinity. The dominant transformation in EPR0 is a decadal diapycnal warming and freshening. A "salinity wall" appears to be reached near 34.6 psu after around 60 years in EPR0. This occurs because the gradual erosion of salinity gradients means that no more salt is available to be transported. The limiting value matches well the volume-averaged salinity, in this latitude and longitude range and down to the ocean floor, in the Levitus (1982) initial state, which is 34.64 psu.

In the depth range 200–400 m (Fig. 13b), a common initial-condition adjustment is again present during the first 5 years. Subsequently, partly shielded from contact with the atmosphere, the transformation in CTRL is largely an isopycnal spiciness increase. Most of the anomalous cooling at this depth (Fig. 7) is in fact seen to be due to a warming of around 1°C in CTRL, from 11.6°C in year 20 to 12.6°C in year 100, and CTRL is apparently still adjusting at year 100. After around 20 years in EPR0, the initially-isopycnal transformation is sharply deflected into a weak diapycnal transformation. Since isopycnal salinity gradients have been significantly eroded by this time (Fig. 11), shutting down the heat flux due to isopycnal mixing (Sect. 3.3), this deflection appears to correspond to the establishment of a new vertical heat balance between upwelling and diffusion.

3.3.5 North–south asymmetry of the thermal adjustment

We finally analyse the thermal adjustment using potential density rather than depth as the vertical co-ordinate (e.g. Speer and Tziperman 1992; Speer et al. 2000). Figure 14 shows the Pacific zonal-mean salinity averaged over the first year of CTRL, calculated as described in the caption. Annual means in other years show the same broad features. The mean salinity, 34.6 psu, has been subtracted, to produce a quantity that may be interpreted as the spiciness. The shape of the ocean surface in density co-ordinates warrants a brief comment. The bulk increase in surface density with increasing distance from the equator is due to the basic meridional surface temperature structure, but the two local surface density minima near the equator (seen as the two peaks in Fig. 14) are due to the surface salinity structure, which displays a freshening under the ITCZ and SPCZ.

The (warm and salty) positive spiciness anomaly in the southern half of Fig. 14 is due to the salty feature associated with the subtropical gyre, seen in Fig. 4a. A key benefit of using density as the vertical co-ordinate is that isopycnal mixing acts "horizontally", allowing its effects to be seen easily. For example, Fig. 14 suggests that, due to the southern positive spiciness anomaly just referred to, the direction of the heat transfer across the thermodynamic bowl (see figure caption) in the CTRL south is *from* the ocean interior *to* the mixed layer. This applies for potential densities in the approximate range 23.0–25.0, for which the isopycnal surfaces outcrop at latitudes in the approximate range 20–35°S. As this heat flux shuts down in EPR0, there is a surface cooling contribution which is much stronger in the south than in the north, since the northern positive spiciness anomaly in Fig. 14 is much weaker than the southern one. This is consistent with the anomalous surface warming in the north being significantly greater than in the south (Fig. 5b).

4 Impacts on the inter-annual variability

Having examined the impacts of the disabled freshwater flux on the mean thermohaline state in Sect. 3, we now briefly examine the impacts on the El Niño/Southern Oscillation (ENSO). Using all 100 model years of both simulations, the mean SST in the Niño-3 region (150°W–90°W and 5°S–5°N) is higher by 0.5°C in EPR0 than CTRL, which is unsurprising given the low-latitude Pacific-wide warming discussed in Sect. 3.2. The mean zonal wind stress in the Niño-4 region (160°E–150°W and 5°S–5°N) is unchanged at 35×10^{-3} N m^{-2}, which is also unsurprising given the discussion of Sect. 2.2.

Power spectra using all 100 years of model data reveal no significant change in the frequency of El Niño events (not shown). The standard deviation of the Niño-3 SST anomaly (with respect to the seasonal cycle) reveals a slight reduction in the amplitude of

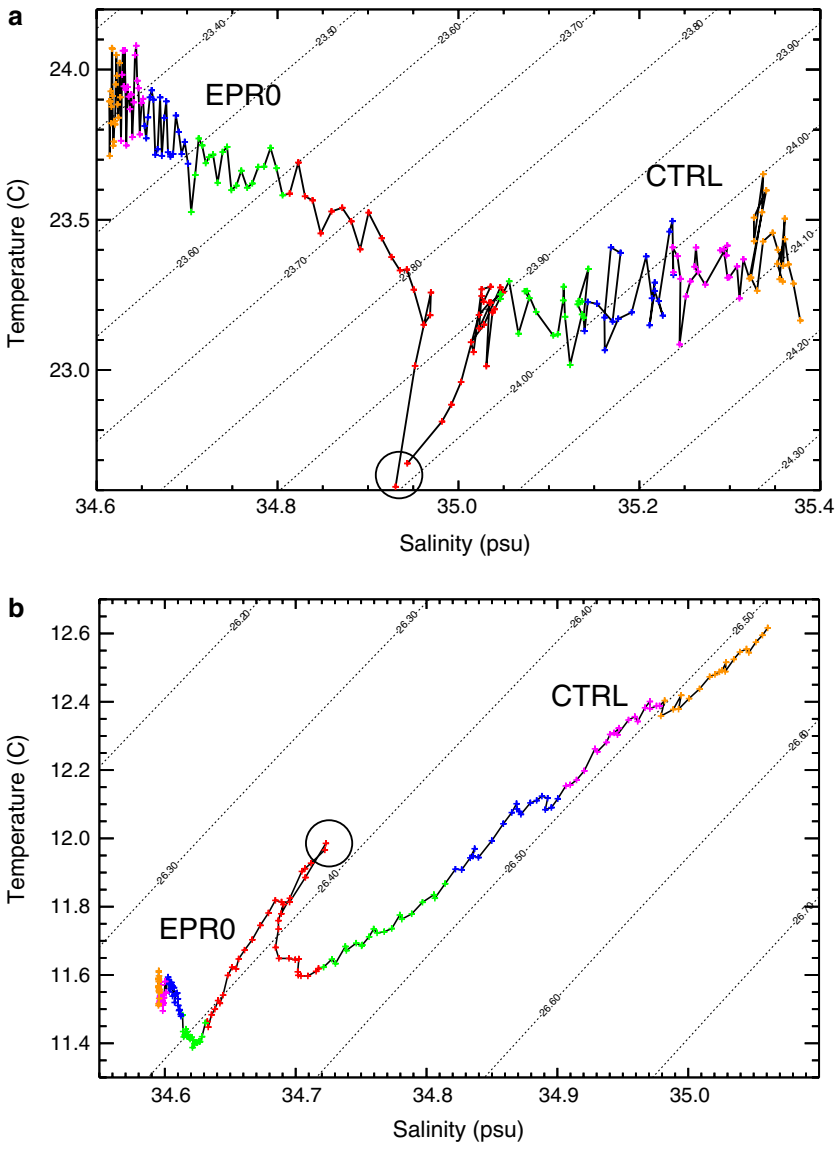

Fig. 13 Trajectories traced out by annual-mean temperature and salinity in the Pacific, for CTRL and EPR0, using depth ranges of **a** 0–100 m, and **b** 200–400 m. In both cases, the latitude and longitude ranges for the averaging are 40°N–40°S and 110°E–70°W. Each point (+) represents one model year: years 1–20 are in *red*, years 21–40 in *green*, years 41–60 in *blue*, years 61–80 in *purple* and years 81–100 in *orange*. The points corresponding to year 1 are *circled*. Contours of constant potential density, σ_0, are shown as *dotted lines*

ENSO, from 0.74°C in CTRL to 0.67°C in EPR0. The inter-annual coupling strength, which is a measure of how strongly the atmospheric winds respond to SST anomalies (Guilyardi 2006), is slightly increased from 6.9×10^{-3} N m^{-2} °C^{-1} in CTRL to 7.4×10^{-3} N m^{-2} °C^{-1} in EPR0.

The fact that El Niño events are almost unaltered by a homogeneous upper-ocean salinity field confirms the minor role played by salinity in the ENSO cycle.

5 Discussion

We have investigated the impacts on the low-latitude Pacific Ocean of a disabling the surface freshwater forcing, using the SINTEX coupled ocean–atmosphere general circulation model. Our attention was restricted to the adjustment of the upper 1,000 m between 40°N and 40°S over 100 years. The surface heat and momentum fluxes are shown to be only slightly affected by the modified freshwater flux. In response to the disabled freshwater forcing, changes to the surface buoyancy, near-surface vertical mixing and mixed-layer depth are established rapidly (i.e. within one year). There then follows a multi-decadal thermal adjustment, consisting of a surface warming which reaches an average of 0.6°C, and a cooling below 200 m which reaches up to 1.1°C. The differences between the control and perturbation integrations are generally large. The changes due to the lack of surface freshwater flux, shown in Figs. 3b, c, 4, 5a, 7, 10, 11a and 13, each clearly exceed the internal variability of the model and are obviously statistically significant by inspection.

The multi-decadal thermal adjustment is achieved by a net transfer of heat from the ocean interior to the upper 200 m. We have presented evidence that the mechanism responsible for this transfer is a gradual shutdown of the along-isopycnal heat flux, whose ver-

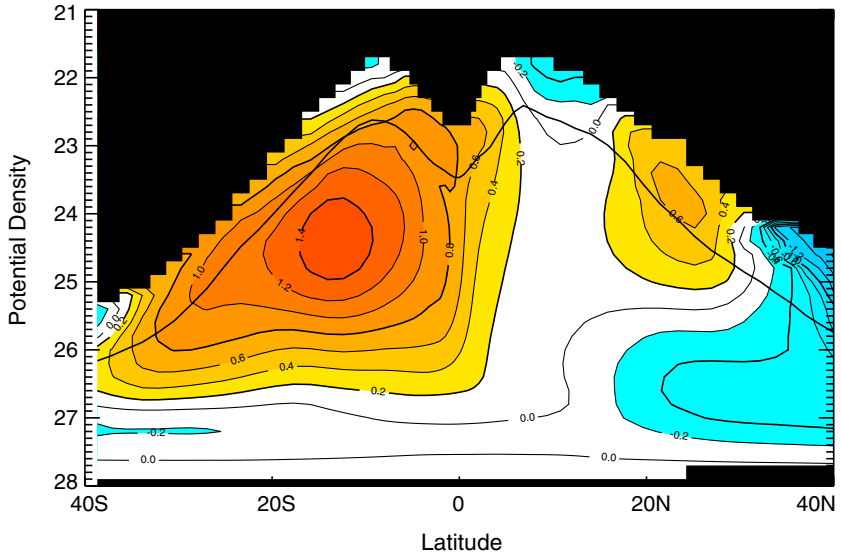

Fig. 14 Annual-mean salinity (psu) in year 1 of the CTRL Pacific Ocean, as a function of potential density and latitude, zonally-averaged over longitudes 110°E–70°W. The mean salinity, 34.6 psu, has been subtracted. Two subtleties arise during the transformation from depth to potential density co-ordinates. First, we must project the monthly-mean thermohaline structure onto the monthly-mean density field, and only then compute the annual mean, in order to capture the seasonal co-variation of the thermohaline structure and the density field. Second, a static instability sometimes (in around 1% of cases) exists in water columns, and so we first pre-condition the model output (to produce monotonic density profiles) by applying the non-penetrative convective adjustment scheme of Madec et al. (1991). The location of the *thermodynamic bowl*, defined to be the maximum depth reached by the mixed layer in the course of a year (Guilyardi et al. 2001), is over-plotted

tical component is directed downwards and has magnitude around 1 W m^{-2} at low latitudes. This heat flux results from the isopycnal mixing of density-compensating temperature and salinity (spiciness) gradients. The timescale for the shutdown of this mechanism is therefore set by the timescale for the decay of isopycnal salinity gradients in response to the eliminated freshwater forcing, which we demonstrate to be around 10–20 years, consistent with the thermal adjustment timescale seen in our experiment. Furthermore, the amplitude of the adjustment is well predicted by a simple heat balance calculation based on the magnitude of the vertical component of the flux.

We now discuss the possible global response to changes in the deep thermohaline circulation, which have recently been shown to have a strong impact in the tropics (Timmermann et al. 2005). In EPR0, the strength of the Atlantic meridional overturning circulation falls from around 20 Sv at the start of the experiment to around 10 Sv after 100 years. This is consistent with a deepening of the global thermocline and an increase in sea surface temperature, which is indeed what is observed in EPR0. However, such an adjustment of the global thermocline cannot explain the cooling observed at depth in EPR0. This would appear to unambiguously rule out changes in the deep thermohaline circulation as the cause of the observed multi-decadal thermal adjustment in our experiments.

We find that the period of the El Niño/Southern Oscillation (ENSO) is not significantly altered by the salinity homogenization, but that its amplitude is slightly reduced (by 10%) compared to that of the control run. This is consistent with the conventional belief that salinity plays a minor role in the ENSO cycle. This finding must be treated with some caution, however. Maes et al. (2002) have reported that the salinity barrier layer may affect the onset of El Niño in a coupled ocean–atmosphere GCM, since the barrier layer influences the build-up of heat in the warm pool. There is an apparent conflict between this finding and our own results, since the salinity barrier layer is removed due to the salinity homogenization in our experiment, and yet the build-up of heat in the warm pool appears to be relatively unaffected. The resolution of this discrepancy may lie in the fact that different models have different El Niño characteristics, and hence different sensitivities to similar changes. In particular, the amplitude and seasonal phase lock of El Niño in the SINTEX model are weak (Guilyardi 2006). This may reduce the sensitivity of the modelled El Niño to the present ocean salinity structure changes.

The key findings of this study are summarized in the flow chart of Fig. 15, which may be regarded as a refined version of the route from *hydrological cycle* to *climate* in the feedback loop depicted in Fig. 1. Although our study has investigated the response of the low-latitude Pacific Ocean to a *disabling* of the hydrological cycle, we may extrapolate the results to speculate about the response to a future *intensified* hydrological cycle, such as that expected to result from global warming. If the centres of net evaporation and net precipitation in Fig. 3a were to intensify, we would expect an increase in isopycnal

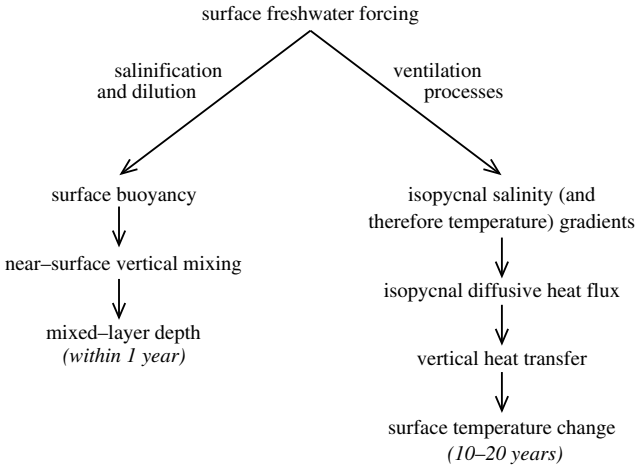

Fig. 15 Flowchart summarizing the mechanisms and timescales with which the low-latitude Pacific Ocean responds to surface freshwater forcing, according to the results of our study

salinity gradients, a corresponding increase in isopycnal temperature gradients, and an increase in the downward low-latitude along-isopycnal heat flux. This would result in an interior warming and a surface cooling. This mechanism would therefore appear to represent a (probably weak) negative sea surface temperature feedback with a multi-decadal timescale, which we speculate might partially shield from view the anthropogenically-forced global warming signal at low latitudes. The implication is that changes in the along-isopycnal heat flux may play a role in determining the climate sensitivity, i.e. the equilibrium global-mean temperature increase resulting from a doubling of atmospheric CO_2. A new sensitivity experiment to investigate these issues, in which the strength of the hydrological cycle is doubled, is currently in progress. We note that the vertical component of the along-isopycnal heat flux is directed *upwards* at high latitudes and that its magnitude is perhaps a factor of ten greater than at low latitudes (Osborn 1998). This suggests a high-latitude feedback which is different, both qualitatively and quantitatively, from the low-latitude feedback discussed in the present study, something that we also plan to investigate in future model runs.

The results of the present study may assist with the development of better climate models, through the identification and understanding of linked systematic errors. In particular, our results show that the surface freshwater flux plays a role in determining ocean temperature structures. Therefore evaporation and/or precipitation biases in GCMs could cause sea surface temperature biases. As noted by Barsugli et al. (2005), most current climate models have trouble simulating tropical rainfall, especially that due to the intertropical convergence zone, and many of these models also exhibit 1–2°C biases in tropical sea surface temperature. If a causal link between these two biases could be demonstrated, then correcting the freshwater bias in models may partially correct the surface temperature bias. If future work reveals this to be the case, then it would provide renewed justification for improving the representation of the hydrological cycle in models.

Acknowledgments Discussions with Pascale Braconnot, Didier Swingedouw, Jean-Claude Dutay, Malcolm Roberts and Thomas Haine were very helpful. Technical model assistance from Daniel Bernie and Silvio Gualdi is gratefully acknowledged. Calculations were performed on the NEC SX-6 at the Deutsches Klimarechenzentrum (DKRZ). We acknowledge funding from the Rapid Climate Change thematic programme of the UK Natural Environment Research Council (award reference: NER/T/S/2002/00442).

References

Allen MR, Ingram WJ (2002) Constraints on future changes in climate and the hydrologic cycle. Nature 419:224–232

Banks HT, Bindoff NL (2003) Comparison of observed temperature and salinity changes in the Indo-Pacific with results from the coupled climate model HadCM3: processes and mechanisms. J Clim 16:156–166

Barsugli J, Shin S-I, Sardeshmukh PD (2005) Tropical climate regimes and global climate sensitivity in a simple setting. J Atmos Sci 62:1226–1240

Barthelet P, Terray L, Valcke S (1998) Transient CO_2 experiment using the ARPEGE/OPAICE non-flux corrected coupled model. Geophys Res Lett 25:2277–2280

Bindoff NL, McDougall TJ (2000) Decadal changes along an Indian ocean section at 32°S and their interpretation. J Phys Oceanogr 30:1207–1222

Bosilovich MG, Schubert SD, Walker GK (2005) Global changes of the water cycle intensity. J Clim 18(10):1591–1608

Braconnot P, Joussaume S, Marti O, de Noblet N (1999) Synergistic feedback from ocean and vegetation on the African monsoon response to mid-holocene insolation. Geophys Res Lett 26:2481–2484

Broecker WS, Peteet DM, Rind D (1985) Does the ocean-atmosphere system have more than one stable mode of operation? Nature 315:21–26

Chahine MT (1992) The hydrological cycle and its influence on climate. Nature 359(6394):373–380

Dai A, Fung IY, Del Genio AD (1997) Surface observed global land precipitation variations during 1900–88. J Clim 10:2943–2962

Delecluse P, Madec G (1999) Ocean modelling and the role of the ocean in the climate system. In: Holland WR, Joussaume S, David F (eds) Modeling the Earth's Climate and its Variability. NATO Advanced Study Institute, Les Houches, 1997, Elsevier Science, pp 237–313

Deser C, Alexander MA, Timlin MS (1996) Upper-ocean thermal variations in the North Pacific during 1970–1991. J Clim 9:1840–1855

Dong BW, Sutton RT (2002) Adjustment of the coupled ocean-atmosphere system to a sudden change in the thermohaline circulation. Geophys Res Lett 29(15):1728

Dufresne J-L, Fairhead L, Le Treut H, Berthelot M, Bopp L, Ciais P, Friedlingstein P, Monfray P (2002) On the magnitude of positive feedback between future climate change and the carbon cycle. Geophys Res Lett 29(10):1405

Fedorov AV, Pacanowski RC, Philander SG, Boccaletti G (2004) The effect of salinity on the wind-driven circulation and the thermal structure of the upper ocean. J Phys Oceanogr 34:1949–1966

Gaffen DJ, Barnett TP, Elliott WP (1991) Space and time scales of global tropospheric moisture. J Clim 4:989–1008

Gualdi S, Guilyardi E, Navarra A, Masina S, Delecluse P (2003a) The interannual variability in the tropical Indian Ocean as simulated by a CGCM. Clim Dyn 20:567–582

Gualdi S, Navarra A, Guilyardi E, Delecluse P (2003b) Assessment of the tropical Indo-Pacific climate in the SINTEX CGCM. Ann Geophys 46(1):1–26
Guilyardi E (2006) El Niño–mean state–seasonal cycle interactions in a multi-model ensemble. Clim Dyn 26:329–348
Guilyardi E, Madec G (1997) Performance of the OPA/ARPEGE-T21 global ocean-atmosphere coupled model. Clim Dyn 13:149–165
Guilyardi E, Madec G, Terray L (2001) The role of lateral ocean physics in the upper ocean thermal balance of a coupled ocean-atmosphere GCM. Clim Dyn 17(8):589–599
Guilyardi E, Delecluse P, Gualdi S, Navarra A (2003) Mechanisms for ENSO phase change in a coupled GCM. J Clim 16:1141–1158
Guilyardi E, Gualdi S, Slingo J, Navarra A, Delecluse P, Cole J, Madec G, Roberts M, Latif M, Terray L (2004) Representing El Niño in coupled ocean-atmosphere GCMs: the dominant role of the atmosphere component. J Clim 17(24):4623–4629
Haine TWN, Hall TM (2002) A generalized transport theory: water-mass composition and age. J Phys Oceanogr 32:1932–1946
Hall A, Manabe S (1997) Can local linear stochastic theory explain sea surface temperature and salinity variability? Clim Dyn 13:167–180
IPCC (2001) Climate change 2001: the scientific basis. Cambridge University Press, Cambridge
Jackett DR, McDougall TJ (1995) Minimal adjustment of hydrographic profiles to achieve static stability. J Atmos Ocean Technol 12:381–389
Levitus S (1982) Climatological atlas of the world ocean. Technical report, National Oceanic and Atmospheric Administration, 1982. NOAA Professional Paper 13
Madec G, Imbard M (1996) A global ocean mesh to overcome the North Pole singularity. Clim Dyn 12(6):381–388
Madec G, Delecluse P, Crepon M (1991) A three-dimensional numerical study of deep-water formation in the northwestern Mediterranean Sea. J Phys Oceanogr 21(9):1349–1371
Madec G, Delecluse P, Imbard M, Levy C (1998) OPA version 8.1 Ocean General Circulation Model reference manual. LODYC/IPSL Technical Report 11
Maes C, Picaut J, Belamari S (2002) Salinity barrier layer and onset of El Niño in a Pacific coupled model. Geophys Res Lett 29(24), 2206
Maes C, Picaut J, Belamari S (2005) Importance of the salinity barrier layer for the buildup of El Niño. J Clim 18(1):104–118
Munk W (1981) Evolution of physical oceanography, chapter Internal waves and small-scale processes. MIT Press, Cambridge, pp 264–291
Murray RJ (1996) Explicit generation of orthogonal grids for ocean models. J Comp Phys 126(2):251–273
Osborn TJ (1998) The vertical component of epineutral diffusion and the dianeutral component of horizontal diffusion. J Phys Oceanogr 28:485–494
Pardaens AK, Banks HT, Gregory JM, Rowntree PR (2003) Freshwater transports in HadCM3. Clim Dyn 21:177–195
Rahmstorf S (1996) On the freshwater forcing and transport of the Atlantic thermohaline circulation. Clim Dyn 12:799–811
Reynolds RW (1988) A real-time global sea surface temperature analysis. J Clim 1:75–86
Roberts MJ, Banks H, Gedney N, Gregory J, Hill R, Mullerworth S, Pardaens A, Rickard G, Thorpe R, Wood R (2004) Impact of an eddy-permitting ocean resolution on control and climate change simulations with a global coupled GCM. J Clim 17:3–20
Roeckner E et al (1996) The atmospheric general circulation model ECHAM-4: model description and simulation of present-day climate. Max-Planck-Institut für Meteorologie report number 218
Russell GL, Miller JR, Rind D (1995) A coupled atmosphere-ocean model for transient climate change studies. Atmos Ocean 33:687–730
Saenko OA, Gregory JM, Weaver AJ, Eby M (2002) Distinguishing the influence of heat, freshwater, and momentum fluxes on ocean circulation and climate. J Clim 15(24):3686–3697
Schmitt RW (1995) The ocean component of the global water cycle. Rev Geophys, pp 1395–1409
Schneider N (2004) The response of tropical climate to the equatorial emergence of spiciness anomalies. J Clim 17(5):1083–1095
Schneider N, Barnett TP (1995) The competition of freshwater and radiation in forcing the ocean during El Niño. J Clim 8:980–992
Schneider EK, Bhatt US (2000) A dissipation integral with application to ocean diffusivities and structure. J Phys Oceanogr 30(6):1158–1171
Spall MA (1993) Variability of sea surface salinity in stochastically forced systems. Clim Dyn 8:151–160
Speer K, Tziperman E (1992) Rates of water mass formation in the north Atlantic ocean. J Phys Oceanogr 22:93–104
Speer K, Guilyardi E, Madec G (2000) Southern ocean transformation in a coupled model with and without eddy mass fluxes. Tellus 52:554–565
Tailleux R, Lazar A, Reason C (2005) Physics and dynamics of density compensated temperature and salinity anomalies. Part I: Theory. J Phys Oceanogr 35:849–864
Timmermann A, An S-I, Krebs U, Goosse H (2005) ENSO suppression due to weakening of the North Atlantic Thermohaline Circulation. J Clim 18:3122–3139
Uppala SM, Kallberg PW, Simmons AJ, Andrae U, da Costa Bechtold V, Fiorino M, Gibson JK, Haseler J, Hernandez A, Kelly GA, Li X, Onogi K, Saarinen S, Sokka N, Allan RP, Andersson E, Arpe K, Balmaseda MA, Beljaars ACM, van de Berg L, Bidlot J, Bormann N, Caires S, Chevallier F, Dethof A, Dragosavac M, Fisher M, Fuentes M, Hagemann S, Holm E, Hoskins BJ, Isaksen L, PA. EM. Janssen, Jenne R, McNally AP, Mahfouf J-F, Morcrette J-J, Rayner NA, Saunders RW, Simon P, Sterl A, Trenberth KE, Untch A, Vasiljevic D, Viterbo P, Woollen J (2005) The ERA-40 re-analysis. Q J Roy Meteor Soc 131:2961–3012
Valcke S, Terray L, Piacentini A (2000) The OASIS coupler user guide Version 2.4. Technical report TR/CMGC/00-10, CERFACS
Vellinga M, Wood RA (2002) Global climatic impacts of a collapse of the Atlantic thermohaline circulation. Clim Change 54(3):251–267
Veronis G (1972) On properties of seawater defined by temperature, salinity and pressure. J Mar Res 30:227–255
Vialard J, Delecluse P (1998a) An OGCM study for the TOGA decade. Part I: Role of salinity in the physics of the western Pacific fresh pool. J Phys Oceanogr 28:1071–1088
Vialard J, Delecluse P (1998b) An OGCM study for the TOGA decade. Part II: Barrier-layer formation and variability. J Phys Oceanogr 28:1089–1106
Vialard J, Menkes C, Boulanger J-P, Guilyardi E, Delecluse P, McPhaden MJ (2001) Oceanic mechanisms driving the SST during the 1997–98 El Niño. J Phys Oceanogr 31:1649–1675
Vialard J, Delecluse P, Menkes C (2002) A modelling study of salinity variability and its effects in the tropical Pacific Ocean during the 1993–1999 period. J Geophys Res 107:8005
Wong APS, Bindoff NL, Church JA (1999) Large-scale freshening of intermediate waters in the Pacific and Indian oceans. Nature 400:440–443
Yeager SG, Large WG (2004) Late-winter generation of spiciness on subducted isopycnals. J Phys Oceanogr 34(7):1528–1547